DOI: 10.1002/ejic.201000742

# Preparation of Mesoporous ZnO/$Zn(OH)_2$ Spheres and Their Replication to High Surface $TiO_2$ Materials

Yong-Kyung Hwang,[a] Tae-Hwan Kwon,[a] Sung Soo Park,[b] Yeo-Joo Yoon,[b] Yong Sun Won,*[b] and Seong Huh*[a]

**Keywords:** Mesoporous materials / Zinc / Titanium / Metal oxides / Photocatalysis

Crystalline mesoporous ZnO/$Zn(OH)_2$ nanocomposite spheres were prepared by a simple method and subsequently used as a hard template for the preparation of amorphous mesoporous $TiO_2$, which showed a very large surface area, 525 $m^2 g^{-1}$. The hydrolytically unstable nature of the ZnO/$Zn(OH)_2$ spheres made the etching process simple and efficient. $Zn_xTi_yO_{x+2y}$ material was also obtained from different etching processes. The large-surface amorphous $TiO_2$ was crystallized above 350 °C, and the surface area decreased to 202 $m^2 g^{-1}$. The crystalline mesoporous $TiO_2$ exhibited a good photocatalytic activity in the decomposition of methyl orange under UV irradiation.

## Introduction

One of the crystalline forms of titania (i.e., anatase) with a large surface area is a key material for photovoltaics, photocatalysis, and other photon-related applications.[1] The high-quality crystalline nature of porous $TiO_2$ is also required for these applications.[2] There are several reports for the preparation of anatase with a decent surface area.[3–5] In general, the mesoporous titania is prepared by using soft liquid-crystal templates such as tetraalkylammonium surfactants, neutral amines, and neutral block copolymers. This approach, however, has a drawback caused by the instability of the final titania product during the calcination step for the removal of organic templates. The surface area of the titania is generally small. For example, mesoporous anatase $TiO_2$ obtained from a conventional liquid-crystal template approach by using a triblock copolymer P123 exhibited a BET surface area of 106 $m^2 g^{-1}$.[2] Further improvement of the preparation only gave a thin film with a surface area of 266 $m^2 g^{-1}$.[3] Application of 1-dodecylamine as template in the synthesis resulted in an amorphous $TiO_2$ with a surface area of 260–390 $m^2 g^{-1}$.[4] Despite these reports on mesoporous $TiO_2$, the preparation of high-quality crystalline $TiO_2$ particles with mesoscale porosity is still challenging.[6]

Herein we report a new preparation method of crystalline mesoporous $TiO_2$ with a surface area of 202 $m^2 g^{-1}$ as well as amorphous $TiO_2$ having a surface area up to 525 $m^2 g^{-1}$. In this new method, we employed mesoporous ZnO/$Zn(OH)_2$ spherical material as a hard template for the sol–gel preparation of $TiO_2$ by using Ti(*i*PrO)$_4$ as precursor. Because of the poor hydrolytic stability of ZnO/$Zn(OH)_2$ as template, it may be suited for the preservation of the mesoporosity and large surface area of $TiO_2$ during the template removal step. The basic surface of the ZnO/$Zn(OH)_2$ template may also be ideal for the hydrolysis and condensation of the Ti(*i*PrO)$_4$ precursor directly on the surface of the ZnO/$Zn(OH)_2$ hard template. Moreover, pure ZnO is a direct band gap material with a variety of applications such as dye-sensitized solar cells,[7] light-emitting diodes,[8] and photocatalysts.[9] An enormous range of applications will also be possible in the form of mesoporous ZnO. In fact, several attempts to prepare porous ZnO have been reported.[10] However, the preparation methods are rather complex and tedious.

## Results and Discussion

We found a facile single-step synthetic route for mesoporous ZnO/$Zn(OH)_2$ spherical particles with high crystallinity, decent surface area, and well-defined mesoporosity. Although the mesoporous ZnO/$Zn(OH)_2$ spheres contain a minor $Zn(OH)_2$ phase, it was revealed that the spherical particles could be successfully used as a good hard template for other nanoporous oxide materials such as $TiO_2$. The mesoporous ZnO/$Zn(OH)_2$ spheres with large surface area were prepared by a modified procedure, which has been developed to prepare ZnO nanorods based on the epitaxial growth of nanorods on the surface of ZnO nanoparticles.[11]

[a] Department of Chemistry and Protein Research Center for Bio-Industry, Hankuk University of Foreign Studies, Yongin 449-791, Korea
Fax: +82-31-330-4566
E-mail: shuh@hufs.ac.kr
[b] Samsung Electro-Mechanics Co. Ltd., Corporate R&D Institute, Suwon, Gyunggi-Do 443-743, Korea
E-mail: yongsun.won@samsung.com

Supporting information for this article is available on the WWW under http://dx.doi.org/10.1002/ejic.201000742.

   

Initially formed $Zn(OH)_2$ could not completely dehydrate into ZnO when the reaction solvent (methanol) contained a certain amount of water (≤ 0.3 wt.-%). Mesoporous ZnO/$Zn(OH)_2$ spheres were formed instead of ZnO nanorods. The mesoporous ZnO/$Zn(OH)_2$ spheres were prepared by dropwise addition of 0.03 M NaOH in methanol to a solution of 0.01 M zinc acetate dihydrate in methanol at 60 °C. Exhaustive preparation attempts indicated that the addition rate of the NaOH solution and a low relative humidity are critical factors for large surface area porous ZnO/$Zn(OH)_2$ spheres. The Brunauer–Emmett–Teller (BET) surface area and pore volume of the ZnO/$Zn(OH)_2$ spheres were 163 $m^2 g^{-1}$ and 0.31 $cm^3 g^{-1}$, respectively. The ZnO/$Zn(OH)_2$ spheres also exhibited well-defined bimodal porosity centered at 3.77 nm and 7.18 nm, respectively, as shown in Figure S1 based on the Barrett–Joyner–Hallenda (BJH) pore size distribution. The smaller pores showed a narrower distribution than the larger mesopores.

Photoluminescence (PL) spectra of the ZnO/$Zn(OH)_2$ spheres are shown in Figure S2. Two sharp peaks were observed at 372 nm (3.33 eV) and 390 nm (3.18 eV) at a laser power of 0.2 mW, and merged at 382 nm (3.25 eV) as the laser power increased to 2 mW. Those two peaks in the UV region are attributed to the free-exciton emission (FX), which are typically observed in ZnO PL spectra at low-temperature measurements.[12,13] Two peaks were merged as the sample was heated with an elevated laser power. However, a deep-level emission associated with an oxygen vacancy in the visible region (ca. 520 nm) was negligible.[14] This indicates that the alkaline hydrothermal system used for the synthesis contains an oxygen source like water molecules on the surface during the growth, giving an "oxidation-hydrothermal" atmosphere. The PL spectra demonstrate that the ZnO substructure in the ZnO/$Zn(OH)_2$ spheres has a high-quality crystallinity with minimum defects.

Figure 1a shows the powder X-ray diffraction (PXRD) patterns of the as-prepared ZnO/$Zn(OH)_2$ spheres and a sample obtained by annealing at 500 °C. The diffraction peaks of both $Zn(OH)_2$ (JCPDS No. 38-0385) and ZnO (JCPDS No. 36-1451) are combined in the XRD patterns of the as-prepared spheres. The diffraction peaks of $Zn(OH)_2$ disappeared completely, and only the peaks of ZnO were materialized by annealing, because the $Zn(OH)_2$ completely converted to ZnO.[15] Considering the fact that the conversion of $Zn(OH)_2$ to ZnO initiates at a temperature of 125 °C, the annealing temperature of 500 °C is high enough to drive the crystallization of the resulting ZnO.[15,16] In accordance, the surface morphology of annealed spheres was drastically changed as shown in Figure S3, and the internal pores of the parent ZnO/$Zn(OH)_2$ spheres collapsed by dehydration of $Zn(OH)_2$ to ZnO during the annealing as suggested by $N_2$ sorption measurements (from 163 $m^2 g^{-1}$ to 16 $m^2 g^{-1}$).

The surface morphology and nanostructures of the ZnO/$Zn(OH)_2$ spheres were characterized by electron microscopic techniques. The scanning electron microscopy (SEM) image in Figure 1b demonstrates a wiggly surface as in coral reef, consisting of nanosized pores and leading to a large

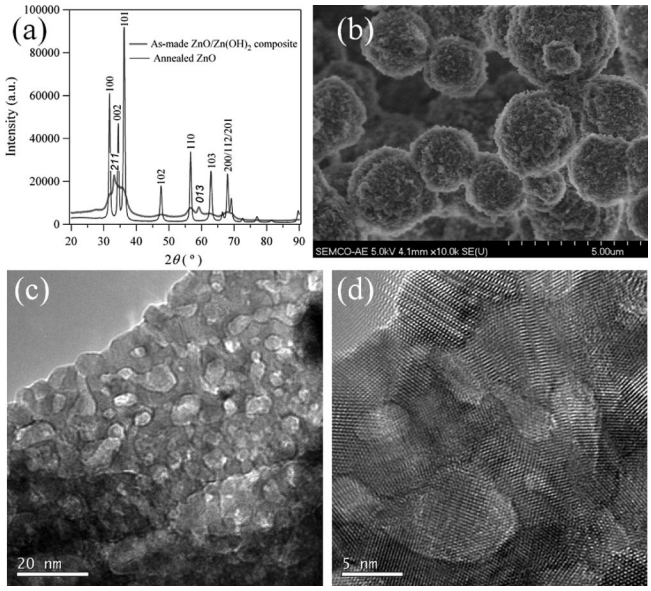


Figure 1. (a) PXRD patterns, (b) SEM image, (c, d) TEM images of the mesoporous ZnO/$Zn(OH)_2$ composite spheres examined under different magnifications.

surface area as confirmed by $N_2$ sorption measurements. A similar morphology has been obtained in an electrochemically grown ZnO nanoporous structure.[16] Energy-dispersive X-ray (EDX) analysis indicated the presence of Zn and O elements (Figure S4). The transmission electron microscopy (TEM) images in Figure 1c and d indicate the highly crystalline nature of the nanoparticles, whose size ranges from 50 to 200 nm in diameter; the nanoparticles lump together to generate porous microstructures. The selected-area electron diffraction (SAED) pattern is shown in Figure S5. The $Zn^{2+}$ ions are supposed to react with NaOH in methanol. Although a certain amount of water is necessary for the control of the growth of ZnO colloidal particles, excess amounts of $H_2O$ hamper the complete condensation of $Zn(OH)_2$ to ZnO.[17] As a result, there is residual $Zn(OH)_2$. The peculiar morphology may also be associated with the excess amount of water, because the zinc species react with water and produce hydrogen bubbles, which prevent smooth deposition and leave behind nanosized pores on the growing surface.[18]

We envisioned that the mesoporous ZnO/$Zn(OH)_2$ spheres might be a good hard template for other porous metal oxides because of their poor hydrolytic stability. Based on this idea, the mesoporous $TiO_2$ was prepared in three steps: an infiltration of the Ti(*i*PrO)$_4$ precursor into the ZnO/$Zn(OH)_2$ spheres at room temperature followed by heat treatment of the $TiO_2$/ZnO/$Zn(OH)_2$ hybrid at 300 °C, and an acid etching of the ZnO/$Zn(OH)_2$ template by a 1.0 M HCl solution. After acid-etching, the template-free amorphous $TiO_2$ was further crystallized into a crystalline form at 350 °C for 24 h ($TiO_2$-350-24). HR-TEM images and SAED patterns confirmed the high-quality crystalline nature of the $TiO_2$-350-24 sample as shown in Figure 3 compared with amorphous $TiO_2$-300-3. On the other hand,

  

a direct crystallization of the $TiO_2$/ZnO/$Zn(OH)_2$ hybrid at 450 °C in air for 3 h followed by acid-etching only afforded $Zn_xTi_yO_{x+2y}$ instead of anatase-rich $TiO_2$ based on PXRD measurements and EDS analysis (Figures S6 and S7). Therefore, it is crucial to etch out the ZnO/$Zn(OH)_2$ template from the $TiO_2$/ZnO/$Zn(OH)_2$ hybrid before crystallization at the optimal temperature. The BET surface area and pore volume of crystalline $TiO_2$-350-24 were 202 $m^2 g^{-1}$ and 0.26 $cm^3 g^{-1}$, respectively (Figures S8 and S9). The phase purity of the sample was confirmed by PXRD as shown in Figure 2c. Neither a rutile nor a brookite phase was observed. A broad single peak at $2\theta$ = 1.88° was observed in the small- angle region as shown in Figure S10.

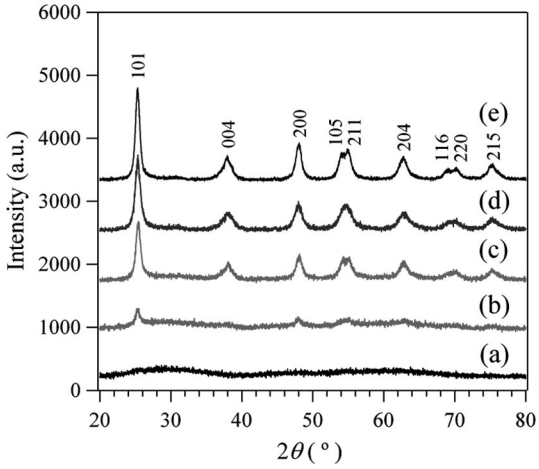


Figure 2. PXRD patterns of mesoporous $TiO_2$ crystallized at different temperatures after an acid-etching process. Anatase-rich $TiO_2$ materials have been obtained above 350 °C after varied periods. (a) 350 °C for 2 h ($TiO_2$-350-2), (b) 300 °C for 72 h ($TiO_2$-300-72), (c) 350 °C for 24 h ($TiO_2$-350-24), (d) 400 °C for 2 h ($TiO_2$-400-2), and (e) 500 °C for 2 h ($TiO_2$-500-2).

The crystallization temperature is an important factor governing the crystalline nature of the final mesoporous $TiO_2$. A sample obtained by heat treatment of the template-free amorphous $TiO_2$ at a lower temperature such as 300 °C for 3 h afforded mesoporous amorphous $TiO_2$ ($TiO_2$-300-3) with a surface area reaching 525 $m^2 g^{-1}$ (Figures S8 and S11). A crystallization of the template-free amorphous $TiO_2$ at higher temperature (500 °C) was not favorable. Only anatase $TiO_2$ with a much lower surface area (65.0 $m^2 g^{-1}$) was obtained based on PXRD and $N_2$ sorption analysis (Figure 2e). These results indicate that the aforementioned crystalline sample $TiO_2$-350-24 may contain a small portion of amorphous $TiO_2$, which we did not quantify. However, the decrease of the surface area upon increase of the crystallization temperature to 500 °C can be mainly attributed to the framework contraction of anatase-rich $TiO_2$-350-24, based on the relative intensity of (101) diffraction peaks of $TiO_2$-350-24 and $TiO_2$-500-2.

Figures 3a and S12 are the TEM images and SAED pattern, respectively, of the amorphous $TiO_2$ after acid-etching. Despite the lack of crystallinity, well-developed mesoscale porosity is clearly discernible. In contrast, the crystallized sample showed well-defined ring patterns indexed as pure anatase as shown in Figure 3b. The particles were consisted of very small spherical nanocrystalline $TiO_2$ particles agglomerated to generate large voids.

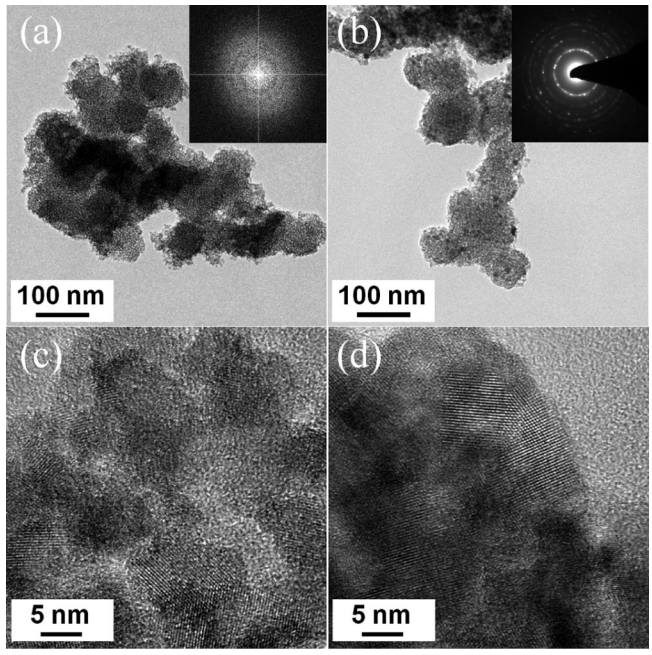


Figure 3. (a) TEM images of amorphous $TiO_2$ ($TiO_2$-300-3) and (b) crystalline $TiO_2$ ($TiO_2$-350-24). Insets are the corresponding SAED patterns. (c, d) HR-TEM images of the crystalline mesoporous $TiO_2$-350-24.

The photocatalytic degradation of methyl orange in an aqueous solution by $TiO_2$-350-24 was investigated under UV irradiation (Figure 4). The methyl orange completely disappeared within 3 h (Figures S13 and S14). Interestingly,

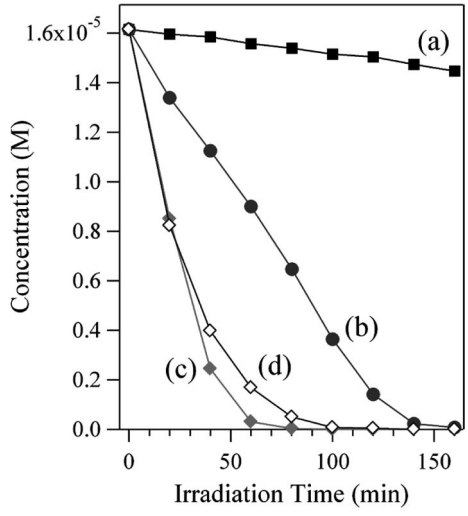


Figure 4. Photocatalytic decomposition profiles of methyl orange catalyzed by crystalline mesoporous $TiO_2$ and Degussa P25 under UV irradiation. (a) Blank run, (b) mesoporous $TiO_2$-350-24, (c) 0.1 M HCl treated $TiO_2$-350-24, and (d) P25.

  

the decomposition rate of methyl orange could be further enhanced with an acid treatment of $TiO_2$-350-24 owing to the exposure of reactive metal centers on the $TiO_2$ surface. Although it is not a fair comparison, we compared the reactivity of $TiO_2$-350-24 with that of Evonik Degussa P25, which contains 25% of rutile phase.[19] The measured BET surface area of P25 was 51.2 $m^2 g^{-1}$. Provided that we used the same mass of the catalysts, the reactivity of $TiO_2$-350-24 is comparable to P25 based on catalyst amount as shown in Figure 4. However, P25 is more active than the acid-treated $TiO_2$-350-24 based on the reactivity per unit surface area. The main reason for the lower reactivity of our mesoporous $TiO_2$-350-24 per unit surface area could be attributable to the different crystallites' surface structures such as particle size and morphology as reported by Balázs et al.[20a] Also the bicrystalline nature of P25 is beneficial to prevent the recombination of photogenerated electrons and holes as reported by Li et al.[20b]

## Conclusions

Highly crystalline mesoporous $ZnO/Zn(OH)_2$ spheres with decent surface area were prepared by a simple single-step method. The spheres were fully characterized by PL studies, gas sorption analysis, and electron microscopy. The hydrolytically unstable nature of the $ZnO/Zn(OH)_2$ composite makes it an ideal hard template for other metal oxides. For example, amorphous $TiO_2$ ($TiO_2$-300-3) with a high surface area of 525 $m^2 g^{-1}$ was obtained after acid-etching of the $ZnO/Zn(OH)_2$ template from the $TiO_2/ZnO/Zn(OH)_2$ hybrid material. This amorphous $TiO_2$ material could be crystallized into an anatase-rich phase with a surface area up to 202 $m^2 g^{-1}$ for $TiO_2$-350-24, which is a good photocatalyst for the decomposition of methyl orange under UV irradiation. Currently, we are exploiting preparations of other catalytically active metal oxides through a $ZnO/Zn(OH)_2$ composite templating approach.

## Experimental Section

**Preparation of Mesoporous $ZnO/Zn(OH)_2$ Spherical Material:** Mesoporous $ZnO/Zn(OH)_2$ spheres were prepared by dropwise addition of a solution of 0.03 M NaOH in methanol (65 mL) to a solution of 0.01 M zinc acetate dihydrate in methanol (125 mL) at 60 °C. The addition rate was about 2 mL/min. The mixture was stirred at 60 °C for 2 h. The white solids were retrieved by centrifugation and washed with distilled water and methanol. The solids were dried at 80 °C for 1 h.

**Preparation of Mesoporous $TiO_2$:** Large surface area amorphous $TiO_2$ was prepared by a nanocasting process using $ZnO/Zn(OH)_2$ as hard template; 1.0 g of $ZnO/Zn(OH)_2$ (pore volume 0.31 $cm^3/g$) was suspended in 10 mL of ethanol with gentle stirring at room temperature for 30 min by using a 40 mL vial. Then 1.0 mL of titanium(IV) isopropoxide [Ti(*i*PrO)$_4$, 3.4 mmol] was directly injected into the solution, and stirring was maintained at room temperature for 48 h. The resulting white $TiO_2/ZnO/Zn(OH)_2$ suspension was filtered, washed with ethanol and dried in air at 80 °C for 1 h. The $TiO_2/ZnO/Zn(OH)_2$ composite was heated in a muffle furnace at 300 °C for 3 h and cooled to room temperature. After thermal treatment, $ZnO/Zn(OH)_2$ was removed by etching with 20 mL of 1.0 M HCl for 1 h. The etched product was filtered and washed with ethanol/$H_2O$ then dried in air at 80 °C for 1 h. In order to obtain mesoporous $TiO_2$ with a crystalline framework ($TiO_2$-350-24), additional crystallization was done at 350 °C in air for 24 h. To prepare an acid-treated $TiO_2$-350-24 sample, 50 mg of mesoporous $TiO_2$-350-24 was treated with 1 mL of 0.1 M HCl (aq), dispersed and shaken for 30 min. Solids were separated by centrifugation (13000 rpm for 10 min) and dried in an oven at 80 °C for 1 h.

**Photocatalytic Decomposition of Methyl Orange:** The photocatalytic activities of the crystalline mesoporous $TiO_2$ samples and P25 (Evonik Degussa Korea) were investigated by monitoring the degradation of methyl orange in an aqueous solution with the as-prepared $TiO_2$ ($TiO_2$-350-24), the acid-treated $TiO_2$-350-24, and P25 under UV irradiation (LC8 UV Spot Light Source, Mercury-Xenon lamp, 200 W, Hamamatsu L9588-01). 45 mL of 0.06 N $TiO_2$ samples were mixed with 750 μL of a 0.001 M methyl orange solution in a quartz flask. UV light was focused on the reaction flask in a darkroom with gentle stirring; 3 mL samples were withdrawn every 20 min from the flask, and absorbances were measured with a UV/Vis spectrophotometer.

**Physical Measurements:** The $N_2$ sorption analysis was performed with a Belsorp-miniII at 77 K (BEL Japan). The samples were dried at 393 K under high vacuum for 2 h. Powder X-ray diffraction patterns were obtained by using a Rigaku MiniFlex (30 kV, 15 mA). FE-SEM images were gathered by using a FEI Nova NanoSEM 200 (10 kV) equipped with an EDAX for EDS spectra. The methanolic suspension of the $ZnO/Zn(OH)_2$ composite was dropped and dried on a Cu grid supported by a holey carbon film for FE-TEM measurements with an FEI Tecnai G2 F20 S-Twin (200 kV) equipped with an HAADF detector and an EDAX. The PL system consisted of a monochromator (Jobin Yvon HR640), a power-adjustable He-Cd laser (KIMMON), and a PMT detector (Hamamatsu C4877).

**Supporting Information** (see footnote on the first page of this article): Detailed preparation methods, gas sorption data, PL spectra, SEM and TEM images, EDX analysis result, and UV spectra during the photocatalysis.

## Acknowledgments

This work was supported by the Hankuk University of Foreign Studies Research Fund of 2010 and the Basic Science Research Program through the National Research Foundation of Korea (NRF) funded by the Ministry of Education, Science and Technology (2010-0010096).

[1] a) H. G. Yang, C. H. Sun, S. Z. Qiao, J. Zou, G. Liu, S. C. Smith, H. M. Cheng, G. Q. Lu, *Nature* **2008**, *453*, 638; b) B. Wu, C. Guo, N. Zheng, Z. Xie, G. D. Stucky, *J. Am. Chem. Soc.* **2008**, *130*, 17563; c) D. Zhang, G. Li, X. Yang, J. C. Yu, *Chem. Commun.* **2009**, 4381.
[2] I. Kartini, D. Menzies, D. Blake, J. C. D. da Costa, P. Meredith, J. D. Richesd, G. Q. Lu, *J. Mater. Chem.* **2004**, *14*, 2917.
[3] T. A. Ostomel, G. D. Stucky, *Chem. Commun.* **2004**, 1016.
[4] Q. Li, P. Härter, W.-M. Xue, J.-L. Zuo, W. A. Herrmann, *J. Chem. Soc., Dalton Trans.* **2001**, 2719.
[5] D. Zhang, L. Qi, *Chem. Commun.* **2005**, 2735.
[6] D. Chen, F. Huang, Y.-B. Cheng, R. A. Caruso, *Adv. Mater.* **2009**, *21*, 2206.
[7] Q.-B. Meng, K. Takahashi, X.-T. Zhang, I. Sutanto, T. N. Rao, O. Sato, A. Fujishima, *Langmuir* **2003**, *19*, 3572.

  

[8] A. Tsukazaki, A. Ohtomo, T. Onuma, M. Ohtani, T. Makino, M. Sumiya, K. Ohtani, S. F. Chichibu, S. Fuke, Y. Segawa, H. Ohno, H. Koinuma, M. Kawasaki, *Nat. Mater.* **2005**, *4*, 42.
[9] N. Kislov, J. Lahiri, H. Verma, D. Y. Goswami, E. Stefanakos, M. Batzill, *Langmuir* **2009**, *25*, 3310.
[10] a) Z. Li, Y. Luan, T. Muc, G. Chena, *Chem. Commun.* **2009**, 1258; b) F. Xu, P. Zhang, A. Navrotsky, Z.-Y. Yuan, T.-Z. Ren, M. Halasa, B.-L. Su, *Chem. Mater.* **2007**, *19*, 5680.
[11] C. Pacholski, A. Kornowski, H. Weller, *Angew. Chem. Int. Ed.* **2002**, *41*, 1188.
[12] L. Wang, N. C. Giles, *J. Appl. Phys.* **2003**, *94*, 973.
[13] Q. Tang, W. Zhou, J. Shen, W. Zhang, L. Kong, Y. Qian, *Chem. Commun.* **2004**, 712.
[14] G. Srinivasan, J. Kumar, *Cryst. Res. Technol.* **2006**, *41*, 893.
[15] H. Kou, J. Wang, Y. Pan, J. Guo, *Mater. Chem. Phys.* **2006**, *99*, 325.
[16] D. R. Lide, *Handbook of Chemistry and Physics*, CRC Press, New York, **1997–1998**.
[17] M. Hasse, H. Weller, A. Henglein, *J. Phys. Chem.* **1988**, *92*, 482.
[18] G.-R. Li, C.-R. Dawa, Q. Bu, X.-H. Lu, Z.-H. Ke, H.-E. Hong, F.-L. Zheng, C.-Z. Yao, G.-K. Liu, Y.-X. Tong, *J. Phys. Chem. C* **2007**, *111*, 1919.
[19] T. Ohno, K. Sarukawa, K. Tokieda, M. Matsumura, *J. Catal.* **2001**, *203*, 82.
[20] a) N. Balázs, D. F. Srankó, A. Dombi, P. Sipos, K. Mogyorósi, *Appl. Catal., B* **2010**, *96*, 569; b) S. Li, Q. Shen, J. Zong, H. Yang, *Mater. Res. Bull.* **2010**, *45*, 882.

Received: July 7, 2010
Published Online: September 22, 2010

  